J Mater Sci: Mater Electron (2013) 24:4643–4654
DOI 10.1007/s10854-013-1456-z

Change of formation velocity of Bi-2212 superconducting phase with annealing ambient

O. Ozturk · G. Yildirim · E. Asikuzun · M. Coskunyurek · M. Yilmazlar · A. Kilic

Received: 21 June 2013 / Accepted: 18 August 2013 / Published online: 28 August 2013

Abstract This exhaustive study enables the researchers to recognize the role of the annealing conditions (temperature and time) on the microstructural, mechanical, electrical and superconducting properties of the Bi-2212 superconducting material with the aid of ρ-T, X-ray diffraction, scanning electron microscopy and Vickers microhardness (H_v) measurements. For this aim, the superconducting samples are elaborated by standard solid-state reaction route at different annealing temperature and different annealing duration. The results show that the annealing temperature of 840 °C and the annealing duration of 72 h are the best for the formation velocity of Bi-2212 superconducting phase. In this study we have focused on microhardness measurements to investigate the mechanical properties. Vickers microhardness, Young's modulus, fracture toughness and yield strength values are calculated separately for all samples. Experimental results of hardness measurements are analyzed using the some models. Finally, the Hays–Kendall model is determined as the most successful model describing the mechanical properties of our samples.

O. Ozturk (✉) · E. Asikuzun · M. Coskunyurek
Department of Physics, Faculty of Arts and Science, Kastamonu University, 37100 Kastamonu, Turkey
e-mail: oozturk@kastamonu.edu.tr

G. Yildirim
Department of Mechanical Engineering, Abant Izzet Baysal University, 14280 Bolu, Turkey

M. Yilmazlar
Faculty of Education, Sakarya University, 54300 Hendek, Sakarya, Turkey

A. Kilic
Department of Physics, Ankara University, 06100 Ankara, Turkey

1 Introduction

During the discovery of Bi-based high temperature superconductors [1, 2] with the general formula $Bi_2Sr_2Ca_{n-1}Cu_nO_y$ (n = 1, 2 and 3), the researchers have been interested in the improvement of their electrical, superconducting, mechanical, microstructural and flux pinning properties by solving the oxygen distribution problem between the active slabs [3–5]. Of the Bi-based superconducting phases, the Bi-2212 phase composed of the double layered cuprate (consecutively stacked layers) is superior to the other phases due to relatively invariant to the oxygen stoichiometry, and especially lesser boundary weak link problems [6–8]. Additionally, grain misorientations and defect interfaces such as grain boundaries, stacking faults, voids, planar and micro defects produce weak or non-superconducting regions, leading to the short coherence length in polycrystalline Bi-2212 superconducting materials [9, 10]. These regions, limiting their direct applications in technology and industry, can also reach the peak point with the presence of the off-stoichiometric dopant like Sr/Bi, Ca/Sr, Ca/Cu and so inhomogeneous distribution of the oxygen content in these slabs affects the crystal structure, electron/mobile hole transport and superconducting properties [11, 12]. To solve this important problem, several methods such as change of the preparation conditions (composition, dopant type and quality), operational procedure, and heat-treatment (time, temperature, atmosphere and pressure) have been studied for last decades. Among them, the heat-treatment plays an important role for the phase formation velocity of the Bi-2212 superconducting matrix because the crystallinity and crystal plane alignments (texturing) have been appeared in the annealing ambient part during the operational procedure. To the best of our knowledge, although there are many papers on the annealing conditions for several materials in

the literature, no detailed reports on the annealing temperature and duration for the formation of Bi-2212 superconducting phase can be found. In the present work, we struggle to report the role of the annealing condition on the electrical, microstructural, mechanical and superconducting properties with the aid of standard measurements such as dc resistivity (ρ-T), X-ray diffraction analysis (XRD), scanning electron microscopy (SEM) and Vickers microhardness (H_v) measurements. Onset-offset critical transition temperature, variation of transition temperature and mobile hole carrier concentration values of all the superconducting samples produced at various annealing ambient are determined from the dc resistivity survey. At the same time, the crystal structure, crystallinity, texturing (crystal plane alignment), phase purity, crystallite size, and lattice parameters are deduced from the XRD researches when the specimen surface morphology, grain connectivity and grain size distribution are inferred from the SEM investigations. Additionally, the microhardness measurements conducted at various indentation loads (0.245 N $\leq$ F $\leq$ 2.940 N) allow us to evaluate the mechanical properties such as Vickers microhardness, elastic modulus, yield strength and fracture toughness of the Bi-2212 superconducting samples studied. Finally, the experimental evidences are analyzed by the available approaches.

2 Experimental details

Precursor powder of Bi-2212 superconducting is provided by Alfa Aesar Co., Ltd. in the high purity of 99.99 %. After mixing in a grinding machine for the duration of 8 h, the homogeneous mixture is filled into cylindrical bar of $6.5 \times 6.5 \times 1$ mm^3 in the air atmosphere and pressed under a force of 7 ton at room temperature. The pellets are subjected to the sintering process at different conditions (in the annealing temperature range of 830–850 °C and time range from 24 to 72 h) to obtain the optimum annealing ambient. In this process, the heating and cooling rates are chosen to be 5 °C min^{-1}. The bulk Bi-2212 superconducting materials prepared in this work are hereinafter presented as A, B, C, D, E (produced at the annealing temperature of 830, 835, 840, 845 and 850 °C for 24 h), F and G (prepared at 840 °C for the annealing duration of 48 and 72 h), respectively.

The electrical resistivity measurements against temperature in a range of 10–120 K are performed in a closed-cycle cryostat at low temperatures down to 3 K by means of the standard dc four-probe technique. The contacts are covered with silver paint for the minimization of the contact resistance. All the measurements are taken by a Keithley 220 programmable current source and a Keithley 2182A nano-voltmeter in the presence of the dc current of 5 mA through the sample inserted in the cryostat with provision for the vacuum. The offset and onset critical transition temperature values belonging to the Bi-2212 superconducting materials are deduced from the resistivity curves. Similarly, the mobile hole-carrier concentration values for each sample are determined theoretically.

The change of the crystal structure, phase impurity, texturing, grain size and lattice parameters of the Bi-2212 superconductors is examined by XRD measurements performed by a Bruker D8 Advance model X-ray diffractometer with the CuKα target, providing a monochromatic beam ($\lambda = 1.54$ Å) in the range of $2\theta = 3°-60°$ in air atmosphere at the room temperature. The precision of crystallite size and cell parameter calculations is about ± 0.01 and ± 0.0001 Å, respectively.

Further, the change of the microstructural analysis due to the annealing ambient is explored by means of a Jeol scanning electron microscope (SEM, JEOL 6390-LV) at the accelerating voltage of 20 kV in the secondary electron image (SEI) mode.

Moreover, a SHIMADZU HVM-2 model digital microhardness tester is used to determine the mechanical properties of the bulk Bi-2212 superconductors. Vickers microhardness (H_v) measurements are exerted on the specimen surface in air atmosphere at the room temperature. The applied indentation test loads are altered from 0.245 to 2.940 N for an applying time of 10 s and the precision of the indentation diagonals is recorded to be about ± 0.1 μm at the different locations on the specimen surface to avoid the surface effects and work hardening. Vickers microhardness, elastic modulus, yield strength and fracture toughness values are discussed clearly. Additionally, the experimental results observed are analyzed by the available models such as Meyer's law, proportional sample resistance model (PSR), modified proportional sample resistance model (MPSR), elastic/plastic deformation (EPD) and Hays–Kendall (HK) approach. The findings are also compared with each others in detail.

3 Results and discussion

3.1 XRD analysis

Phase analysis, texturing (crystal plane alignment), interplaner distance, grain size and cell parameters can easily be analyzed by the diffraction patterns belonging to a superconducting material. Figure 1 gives the room temperature powder XRD patterns between 3° and 60° for the superconductor ceramics, exposed to the different annealing conditions. The characteristic peaks identifying with Bi-2212 phase are displayed by (h k l) Miller indices on the graphs. The absence of any different cationic/anionic phases in the XRD patterns also verifies that the

superconducting phases are taken place thoroughly in the structures. Moreover, the phase formation velocity (determined from the diffraction line intensities) of the Bi-2212 superconducting matrix enhances with the increase of the annealing temperature up to 840 °C above which the phase tends to retrograde considerably and in fact obtains the minimum value as a result of the decrement in the diffraction line intensities. It is necessary to underline that the excess annealing temperature not only damages the Bi-2212 phase but is favorable formation velocity of the Bi-2201 phase, as well. On the other hand, the characteristic peak intensities increase with the annealing duration at the annealing temperature of 840 °C, confirming that the crystallinity and crystal plane alignments of the superconducting samples improve significantly (Fig. 1). The effect of the peak intensities is fairly observed on the superconducting properties of the samples produced in this work. The relative percentages belonging to Bi-2212 and Bi-2201 phases are calculated by the following Eqs. 1, 2, and the findings obtained are listed in Table 1.

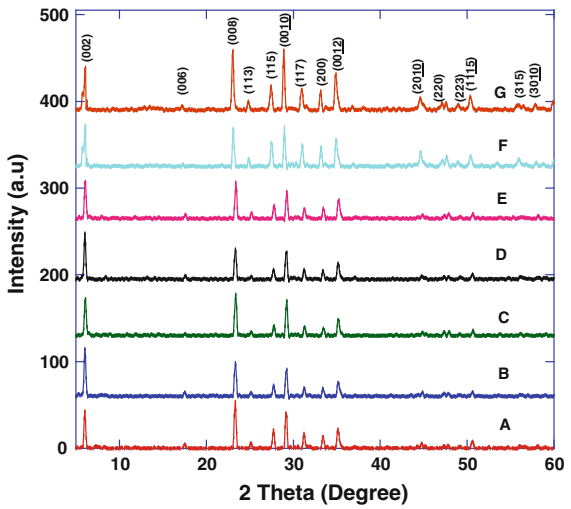

Fig. 1 XRD patterns of the all samples

$$f_{(2212)} = \frac{\sum I_{H(hkl)}}{\sum I_{H(hkl)} + \sum I_{L(hkl)}} \quad (1)$$

$$f_{(2201)} = \frac{\sum I_{L(hkl)}}{\sum I_{H(hkl)} + \sum I_{L(hkl)}} \quad (2)$$

where I is related to the peak intensity of the current phase. One can see from the table that the G sample obtains the maximum Bi-2212 phase percentage while the lowest value of 72 % belongs to the E sample. According to these results obtained, the best annealing ambient is found to be 840 °C for 72 h to produce the formation of Bi-2212 phase. At the same time, the XRD curves enable us to find the lattice constant parameters (a and c) by the least square method in terms of the tetragonal unit cell structure and then discuss the superconducting variation with the reasons. The cell parameters computed are gathered in Table 1. As seen from the table that the largest c parameter (31.33 Å) is observed for the G sample whereas the E sample has the minimum c value of 30.02 Å. Conversely, the largest and smallest a values are attributed to the former and latter samples, respectively. This may be associated with the inhomogeneities in the oxygen concentration, leading to variations (degrade or improvement) in both the structural parameters [13] and superconducting properties of the samples studied.

3.2 Grain size calculation by Scherrer–Warren equation

Grain size calculation is another important result inferred from the XRD patterns as a consequence of the nature of broad peak pointing out the nanocrystalline formation. The grain size belonging to each sample is computed with the aid of the following relation given below [14, 15].

$$t = {}^{0.941\lambda}/_{B\cos\theta_B} \quad (3)$$

where λ is related to the wavelength of the XRD source, t shows the crystal thickness, θ_B denotes the Bragg angle, the peak of which takes place the full width at half maximum (FWHM) of the Bragg peak and is indicated B. Moreover, B is clearly defined as:

Table 1 XRD and electrical resistivity measurement results for the samples

Samples	c (Å)	a (Å)	Volume fracture %Bi-2212 − %Bi-2201	Grain size (Å)	T_c^{onset} (K)	T_c^{offset} (K)	ΔT_c (K)
A	30.08	5.41	76 − 24	79.271	80.85	64.41	16.44
B	30.41	5.39	84 − 16	82.556	82.34	71.41	10.93
C	30.54	5.37	89 − 11	95.201	83.51	75.26	8.25
D	30.23	5.38	83 − 17	80.616	81.86	69.59	12.27
E	30.02	5.43	72 − 28	71.713	77.87	58.16	19.71
F	30.69	5.37	91 − 9	101.547	84.11	76.41	7.70
G	31.33	5.35	95 − 5	107.868	84.79	78.90	5.89

$$B^2 = B_m^2 - B_s^2 \quad (4)$$

where B_s demonstrates the half width of the standard material in radians. The grain sizes determined with regard to the equations are depicted in Table 1. It is visible from the table that the grain sizes calculated increase with the enhancement of the annealing temperature up to the certain annealing temperature of 840 °C beyond which the size tends to decrease systematically and in fact reach to the local minimum point at the sintering temperature of 850 °C. On the other hand, the grains size raises monotonously with the increment of the annealing time. Thus, the maximum grain size (minimum resistivity) of 107.868 Å is observed for the sample annealed at 840 °C for 72 h whereas the minimum point is obtained to be about 71.713 Å for the E sample. This is attributed to the fact that the excess annealing temperature damages the electrical and superconducting properties due to the degradation of the crystallinity and connectivity between the superconducting grains, being favored by the SEM images.

3.3 SEM analysis

Microstructural properties of the bulk Bi-2212 materials are investigated by the SEM in the SEI mode at 5,000× magnification and the images obtained are displayed in Fig. 2. As seen from the figure, similar to the superconducting properties, the crystal size and connectivity between the superconducting grains in the Bi-2212 superconducting samples initially improve with the annealing temperature up to 840 °C after this point both characteristics suppress considerably and in fact they reach the minimum point for the annealing temperature of 850 °C. As for the annealing duration, the surface quality increases regularly with the enhancement of the time up to 72 h. According to these results, the smoothest and densest surface with a fine connectivity between the superconducting grains in the formation of the platelet-like structure (the basic characteristics of Bi-2212 phase formation) [16, 17]. At the same time, it is noted that the G sample has more uniform surface appearance with broader crystal distribution (lower porosity, better texturing, crystallinity and connectivity between the superconducting grains) as compared to the other samples. This is related to the fact that among the samples produced in this study only the G sample exhibits completely the basic characteristics of Bi-2212 superconducting phase. These findings are totally parallel with the XRD evidences.

3.4 Electrical resistivity results

In order to explain the role of the annealing ambient on the critical transition temperatures of the Bi-2212 materials, variation of the dc resistivity against the temperature in the range of 40–105 K is graphically depicted in Fig. 3. As seen from the figure, each sample obtaining a sharp or broad transition to the superconducting state exhibits the metallic behavior above its superconducting onset temperature (T_c^{onset}) values with the positive temperature coefficient of the resistivity. The metallic behavior (linear temperature dependence of resistivity) stems from the electron–phonon interaction (scattering of electrons by the lattice vibrations) in the superconducting structure [18, 19] or logarithmic divergence in density of states at the Fermi level [20–22].

It is another probable result deduced from the figure that both the onset (T_c^{onset}) and offset (T_c^{offset}) critical transition temperatures belonging to the samples tend to increase with the enhancement of the annealing temperature until a certain level of 840 °C above which they begin to decrease considerably and in fact reach to their minimum points for the annealing temperature of 850 °C. Here, the abbreviation terms, T_c^{onset} and T_c^{offset}, are in corresponding to the transition of isolated grains (intra-granular component) to the superconducting state, and volume fraction of the basic phase or inter-granular component, respectively [23, 24]. The maximum T_c^{onset} of 83.51 K and T_c^{offset} of 75.26 K get obtained for the C sample, whereas the E sample has the smallest values (Table 1).

The decrement in the critical temperatures are associated with not only the degradation of the grain size and the mobile hole concentration but the enhancement of the porosity, grain misorientations and defects (stacking faults, voids, planar and micro defects), as well [25, 26]. Distortion between Bi-2212 slabs and possible alterations in the lattice vibration based on the formation of secondary phases may be another reason of the reduction in the T_c^{onset} and T_c^{offset} values [27–30]. The variation denoted as $\Delta T_c(T_c^{onset} - T_c^{offset})$ is another interesting finding for this present study. The results observed indicate that the ΔT_c value decreases systematically with the increase of the annealing temperature up to 840 °C after which the value increases continuously to its maximum point of 19.71 K (for the E sample) due to the increase in the grain boundary weak-links, porosity, grain boundary resistivity [27, 28] and especially the presence of inhomogeneities in the oxidation states of the superconducting grains [13]. The intergrowth of different phases in grains may also be in charge of the enhancement of the variation [31]. As for the annealing time effect, both the T_c^{onset} and T_c^{offset} values monotonously increase from 83.51 to 84.79 K and 75.26 to 78.90 K, respectively. The maximum values are attributed to the G sample. This increment in the critical transition temperatures is related to the optimization of the mobile hole carrier concentration and improvement in the crystallinity and grain size [32]. The long and short of it that the optimum annealing condition is determined to be 840 °C

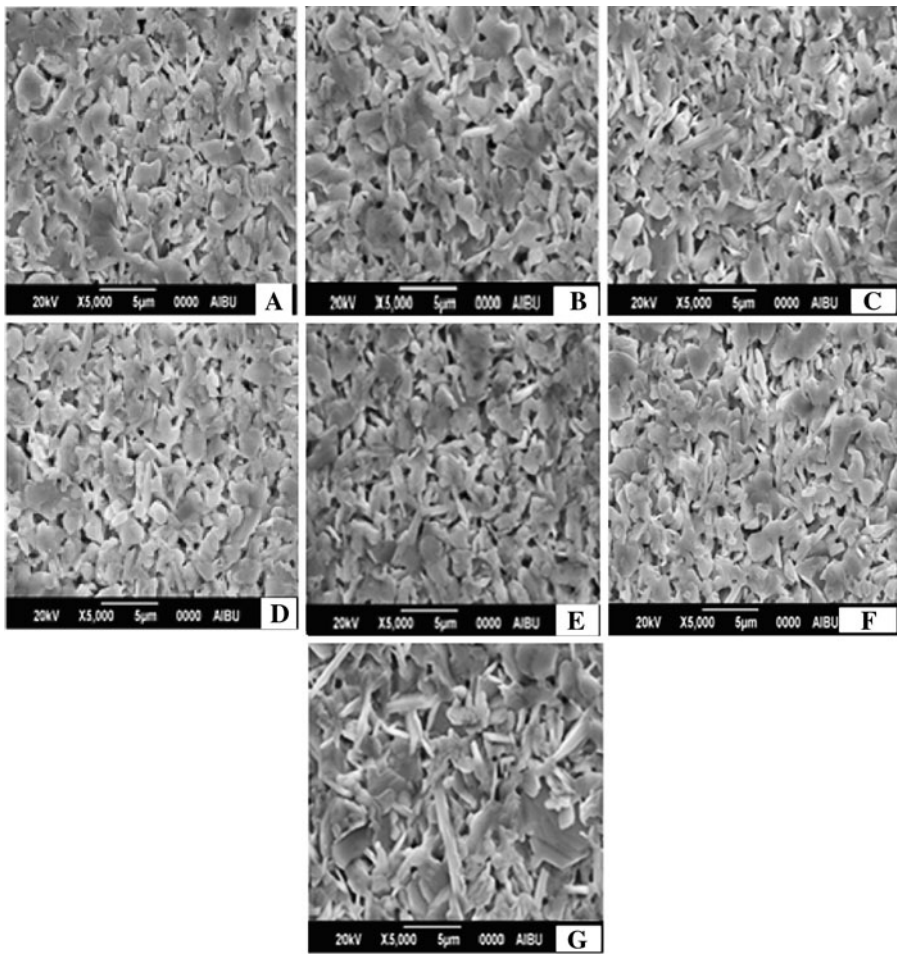

Fig. 2 SEM micrographs of the Bi-2212 superconducting samples

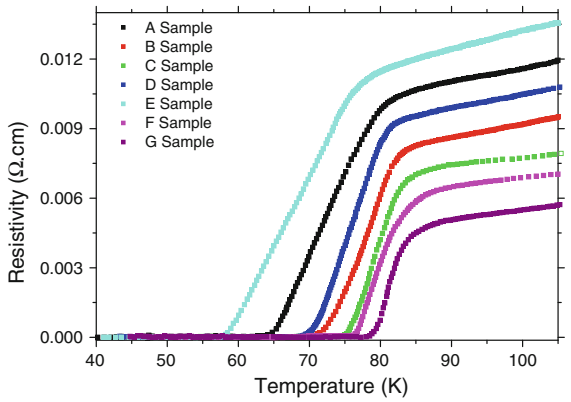

Fig. 3 Variation of resistivity against temperature for the samples studied

for the duration of 72 h to produce the bulk Bi-2212 superconducting material, which is one of the most striking point of this comprehensive paper.

3.5 Vickers microhardness analysis

The Vickers microhardness measurements including the change of the diagonal length over an applied indentation test load are conducted to examine the mechanical characteristics of the bulk Bi-2212 superconducting materials produced at different annealing ambient by the conventional solid-state reaction route. It is customary to say that the cuprate superconductors have the inherit brittleness nature, thus the description of the mechanical performances is important for their technological and industrial applications. At the same time, the Vickers microhardness measurements allow the researchers to find out the elastic (Young's) modulus (E), yield strength (Y) and fracture toughness (K_{IC}) parameters, which are responsible for the potential application of the materials and can be calculated from the following relations in the applied load range of 0.245–2.940 N.

$$H_V = 1,854.4\left(\frac{F}{d^2}\right) \tag{5}$$

$$E = 81.9635H_V \tag{6}$$

$$Y \approx \frac{H_V}{3} \tag{7}$$

$$K_{IC} = \sqrt{2E\gamma} \tag{8}$$

here, γ is attributed to the surface energy. According to the equations, the findings calculated are listed in Table 2. As seen from the table, all the calculated values decrease with the enhancement of the annealing temperature up to the annealing temperature of 840 °C beyond which they systematically decrease towards to the minimum points (Fig. 4a). As for the annealing time, the microhardness parameters extracted decrease with the duration as a consequence of the improvement of the crystallinity and especially the strength of connection between the superconducting grains (Fig. 4b). Shortly, the best mechanical performance is observed for the sample annealed at 840 °C for the annealing duration of 72 h. It is another probable result that all the parameters tend to decrease with the increment in the applied indentation load. This is attributed to the fact that the samples exhibit the indentation size effect (*ISE*) behavior [33, 34]. In other words, the hardness parameters are strongly dependent upon the applied load [35, 36]. Moreover, reverse indentation size effect (*RISE*) is also another sample behavior against the applied indentation test load [37–39]. The basic difference between these available models is due to the surface energy value [40]. The mechanical properties are also examined by Meyer's law, PSR model, MPSR model, EPD and HK approach.

3.5.1 Meyer's law

Meyer's law is an available model to understand the ISE and RISE behavior of a material and identified by the formula given below [41]:

$$F = Ad^{n_K} \tag{9}$$

where the power n is attributed to the Meyer number and A is in corresponding to the standard microhardness constants. With the aid of the Meyer's law, we can experimentally explain the relationship between the applied indentation test load and the indentation diagonal length. Here, the power n enables us to determine the mechanical characteristic (*ISE* and *RISE* behavior) of the sample studied. The Meyer number obtains 3 different scales such as $n_K < 2$ (typical *ISE* feature), $n_K > 2$ (*RISE* behavior) and $n_K = 2$ (Kick's law). For $n_K < 2$, the microhardness values tend to decrease with the increment of the applied load. As for n > 2, the microhardness values increase with the enhancement of the load applied or vice versa. At the last state $n_K = 2$, the Meyer's law gives place to Kick's law, $F = Ad^2$, meaning that the microhardness values are independent on the applied indentation load [42, 43]. For the bulk Bi-2212 superconducting samples prepared in this work, Fig. 5 gives the linear variations of lnF with regard to lnd. Based on the linearity, the n_K values for the samples are deduced from the slopes of the curves (Table 3). It is found that all the n values obtained are smaller than 2, pointing out that the bulk Bi-2212 materials prepared exhibit the typical *ISE* behavior (inverse dependence on the applied load). It is another interesting point extracted from the table that the power n of the sample A is found to be greatest ($n_K = 1.97$) value; or the closest value to 2. This is attributed to the fact that the microhardness values are less affected by the applied load as compared to the others. In other words, it is possible to say that among the Bi-2212 superconductors produced, the A sample is more damaged by the applied indentation load.

Table 2 The calculated load dependent H_v, E, Y and K_{IC} for the samples

Samples	F(N)	H_v (GPa)	E (GPa)	Y (GPa)	K_{IC} (Pa/m$^{1/2}$)
A	0.245	0.589	48.27	0.196	250.28
	0.490	0.580	47.53	0.193	248.36
	0.980	0.571	46.80	0.190	246.44
	1.960	0.566	46.39	0.188	245.36
	2.940	0.560	45.90	0.186	244.06
B	0.245	0.576	47.21	0.192	263.59
	0.490	0.555	45.49	0.185	258.75
	0.980	0.550	45.08	0.183	257.58
	1.960	0.543	44.50	0.181	255.92
	2.940	0.541	44.34	0.180	255.45
C	0.245	0.546	44.78	0.182	358.22
	0.490	0.536	43.98	0.178	355.00
	0.980	0.507	41.60	0.169	345.27
	1.960	0.495	40.62	0.165	341.20
	2.940	0.488	40.01	0.162	338.61
D	0.245	0.448	36.79	0.149	213.77
	0.490	0.430	35.31	0.143	209.48
	0.980	0.425	34.85	0.141	208.05
	1.960	0.422	34.62	0.140	207.36
	2.940	0.418	34.31	0.139	206.43
E	0.245	0.437	35.83	0.145	184.71
	0.490	0.423	34.73	0.141	181.85
	0.980	0.420	34.45	0.140	181.12
	1.960	0.417	34.22	0.139	180.50
	2.940	0.414	33.99	0.138	179.89
F	0.245	0.508	41.70	0.169	268.07
	0.490	0.465	38.15	0.155	256.41
	0.980	0.454	37.24	0.151	253.33
	1.960	0.452	37.56	0.152	254.42
	2.940	0.450	36.94	0.150	252.30
G	0.245	0.434	35.57	0.144	272.13
	0.490	0.417	34.17	0.139	266.72
	0.980	0.397	32.53	0.132	260.24
	1.960	0.392	32.12	0.131	258.59
	2.940	0.390	31.96	0.130	257.95

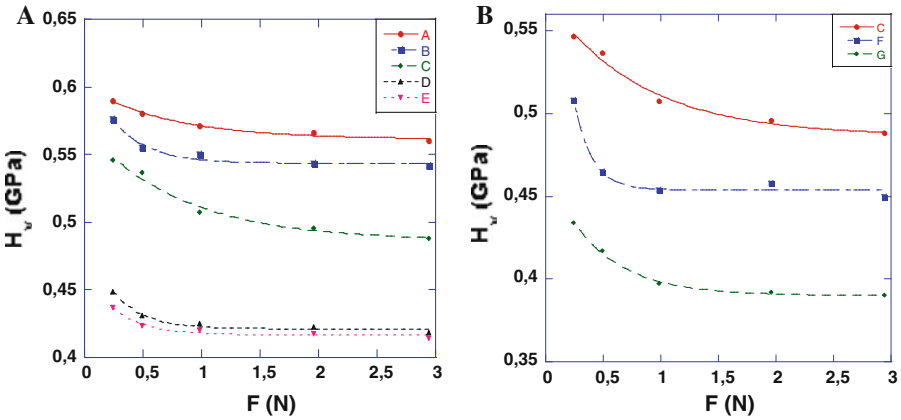

Fig. 4 Variations of microhardness over the applied indentation test load for **a** the materials annealed at various temperatures for 24 h and **b** the samples exposed to the annealing process at 840 °C for different durations

3.5.2 *Analysis of PSR model*

In 1993, Li and Bradt propounded the PSR model that is one of the reliable and useful approaches to describe the mechanical characteristics of a material [44]. This model is also thought as the modification of Hays–Kendall approach and the sample resistance changes linearly with the indentation diagonal length. The mechanical behavior, *ISE* or *RISE*, of a material is determined with the aid of following relation,

$$F = \alpha d + \beta d^2 \tag{10}$$

where the surface energy parameter is depicted by α, variation of which is associated with the energy dispersion of the surface cracks. α and β parameters are inferred from the linear graphs of *F/d* versus *d* (Fig. 6). Li and Bradt [44] declare that these parameters are directly related with the plastic (irreversible) and elastic (reversible) deformation of the material. In particular, the parameter of β is asserted to be a measurement of the real (true) microhardness and allows us to find the load independent (H_{PSR}) microhardness by means of the formula given below:

$$H_{PSR} = 1,854.4\beta \tag{11}$$

It is apparent from Table 4 that all the α parameters are found to be positive for the bulk Bi-2212 samples exhibiting the *ISE* behavior. In other words, both the elastic (reversible) and plastic (irreversible) deformations are

Table 3 Best-fit results of experimental data based on Meyer's law

Samples	n_k	$\ln_{A1k}$ (GPa)
A	1.97	−7.92
B	1.95	−7.92
C	1.90	−7.81
D	1.95	−8.07
E	1.96	−8.22
F	1.92	−7.97
G	1.92	−8.07

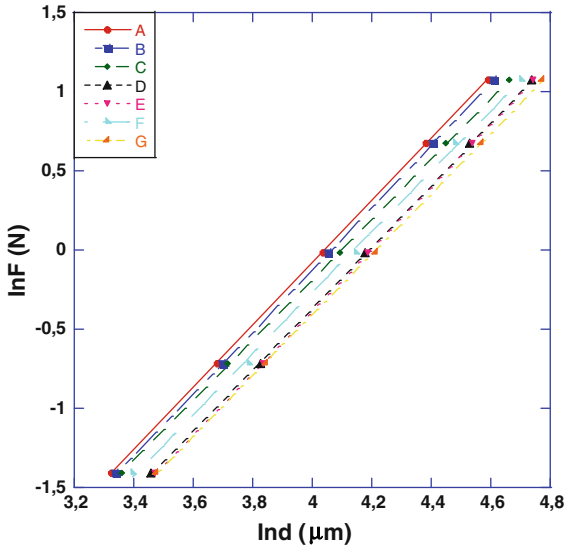

Fig. 5 Change of applied load ln *F* with diagonal ln *d* for the samples

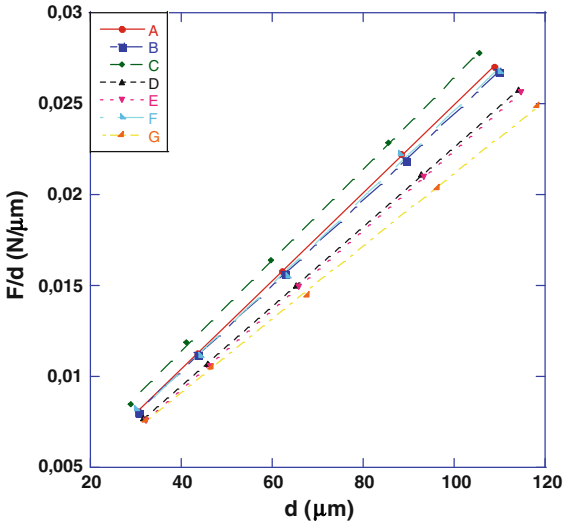

Fig. 6 Plots of F/*d* versus *d* for the samples

Table 4 Best-fit results of experimental data according to *PSR* model

Samples	$\alpha \times 10^{-5}$ (N/μm)	$\beta \times 10^{-5}$ (N/μm^2)	Load independent H_{PSR} (GPa)	Load dependent H_v (GPa)
A	64.89	29.54	0.547	0.560–0.566
B	73.59	25.86	0.479	0.541–0.543
C	143.27	25.01	0.463	0.488–0.495
D	62.10	22.04	0.408	0.418–0.422
E	47.60	21.96	0.407	0.414–0.417
F	86.16	23.69	0.439	0.450–0.458
G	104.10	20.06	0.371	0.390–0.392

simultaneously produced in the pure Bi-2212 superconducting samples. One can see the determined H_{PSR} values in Table 4. Based on the results obtained, the PSR model is not successful enough to describe the mechanical characteristics due to the fact that the original (load independent) microhardness values are far from the plateau region for the samples studied [45, 46]. Moreover, the original elastic modulus (E), yield strength (Y) and fracture toughness (K_{IC}) values are calculated from the load independent H_{PSR} values with the aid of Eqs. 6–8 and the values computed are embedded in Table 5. It is visible from the table that the real values (E_0, Y_0 and K_{IC}) decrease as compared to the load dependent values. At the same time, the G sample obtaining the best superconducting and microstructural properties exhibits the lowest microhardness values, confirming that the annealing condition of 840 °C for 72 h improves the connectivity between superconducting grains. The similar findings can be found in [36, 45].

3.5.3 Analysis of MPSR model

This model, studied for the modification of the *PSR* approach, is more useful to examine the materials obtaining *ISE* nature instead of the *RISE* nature. The indentation diagonal length is calculated from the following relation [47].

$$F = W_{MPSR} + A_{0MPSR}d + A_{1MPSR}d^2 \quad (12)$$

According to the current model calculation, the physical meanings of the A_{0MPSR} and A_{1MPSR} parameters are the similar with the *PRS* model (Fig. 7). However, any damage/break/void can appear on the specimen surfaces during the sample preparation procedure. Thus, the load independent microhardness values can be calculated from the following equation.

$$H_{MPSR} = 1,854.4A_{1MPSR} \quad (13)$$

All the calculated values such as W_{MPSR}, A_{0MPSR} and A_{1MPSR} can be found in Table 6. It is visible from the table that although the *MPRS* findings are computed to be closer to the saturation region than those of the *PRS* approach, they are even far from the real microhardness values.

Table 5 The calculated load independent H_0, E_0, Y_0 and K_{IC} values belonging to the samples

Samples	H_0 (GPa)	E_0 (GPa)	Y_0 (GPa)	K_{IC} (Pa/m$^{1/2}$)	H_v (GPa)
A	0.547	44.83	0.182	241.20	0.560–0.566
B	0.479	39.26	0.159	240.38	0.541–0.543
C	0.463	37.94	0.154	329.75	0.488–0.495
D	0.408	34.44	0.136	203.80	0.418–0.422
E	0.407	33.35	0.135	178.21	0.414–0.417
F	0.439	35.98	0.146	249.00	0.450–0.458
G	0.371	30.40	0.123	250.33	0.390–0.392

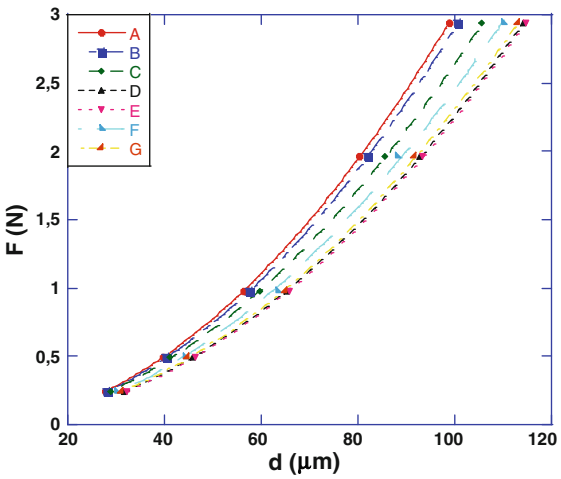

Fig. 7 Variation of applied load with the indentation diagonal length for the samples

Based on the important result, it is not wrong to say that the *MPRS* model is insufficient to explain the mechanical properties of the Bi-2212 superconductors produced.

3.5.4 Analysis of EPD model

Elastic/plastic deformation (*EPD*) model is another method to characterize the mechanical properties and behavior (*ISE*

Table 6 Best-fit results of experimental data based on *MPSR* model

Samples	W_{MPSR} (N)	$A_{0MPSR} \times 10^{-5}$ (N/μm)	$A_{1MPSR} \times 10^{-5}$ (N/μm^2)	Load independent H_{MPSR} (GPa)	H_v (GPa)
A	0.025	166.69	28.70	0.532	0.560–0.566
B	0.069	41.72	28.61	0.530	0.541–0.543
C	0.014	200.36	24.56	0.455	0.488–0.495
D	0.0004	62.03	22.05	0.408	0.418–0.422
E	0.0024	55.08	21.91	0.406	0.414–0.417
F	0.028	180.56	23.03	0.427	0.450–0.458
G	0.028	5.60	20.74	0.384	0.390–0.392

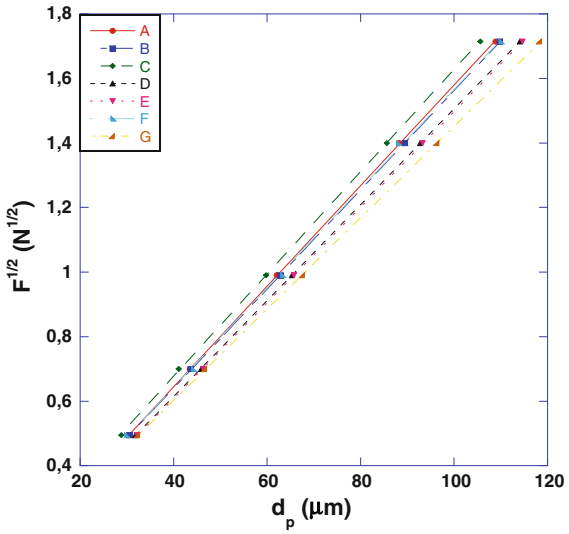

Fig. 8 Plots of diagonal length versus square root of applied loads for the samples

Table 7 Best-fit results of experimental data according to *EPD* method

Samples	A_2 (N/μm^2)	d_e (μm)	H_{EPD} (GPa)	H_v (GPa)
A	0.017	0.018	0.535	0.560–0.566
B	0.016	0.020	0.474	0.541–0.543
C	0.015	0.043	0.464	0.488–0.495
D	0.014	0.020	0.408	0.418–0.422
E	0.014	0.065	0.407	0.414–0.417
F	0.015	0.026	0.439	0.450–0.458
G	0.014	0.035	0.363	0.390–0.392

and *RISE*) under the applied load of a sample. In the classic microhardness measurements, the indentation diagonal length is determined after removing the applied indentation load. In this model, the elastic recovery appears in the vicinity of the indentation track. In this respect, the indentation diagonal shrinks towards to the certain point, thus the true microhardness values are determined with the addition of a new term in the diagonal length [48]. Namely,

$$F = A_2(d_e + d_p)^2 \tag{14}$$

where A_2 is the real microhardness constant when the d_e and d_p are attributed to the elastic and plastic (correction term) deformation, respectively. The A_2 and d_e parameters evaluated from the linear graphs of $F^{1/2}$ versus d_p (Fig. 8) are tabulated in Table 7 in detail. As seen from the table that all the extrapolated d_e values are found to be positive as a result of the ISE behavior, meaning that the plastic deformation as well as the elastic deformation plays dominant role due to the elastic recovery in the materials [49]. If the irreversible deformation is more dominant in the material instead of the reversible deformation, the value of d_e will be obtained to be negative due to the Reverse Indentation Size Effect (*RISE*) behavior [50]. This means that the microhardness values increase with the enhancement of the applied indentation load [51, 52]. At the same time, this model lets us find the load independent microhardness value by the following equation:

$$H_{EPD} = 1,854.4A_2 \tag{15}$$

The results computed are displayed in Table 7. As seen from the table that the maximum H_{EPD} value of 0.535 GPa is observed for the sample annealed at 830 °C for 24 h, verifying that among the samples, this one exhibits the worst mechanical properties. Nevertheless, none of the load H_{EPD} values are calculated to be close to the saturation region (real microhardness values) for the superconducting samples prepared. Thus, this model, similar to the Meyer's law, PSR and MPSR, is not sufficient to explain the true mechanical properties of the Bi-2212 superconducting samples studied in this work.

3.5.5 Analysis of Hays–Kendall approach

Hays–Kendall approach is one of the most reliable and useful descriptor for the mechanical properties of the superconducting materials obeying the ISE feature. In this model, there is a certain limit of test load (W) called as critic point after which the plastic (irreversible) deformation begins to be much more dominant than the elastic

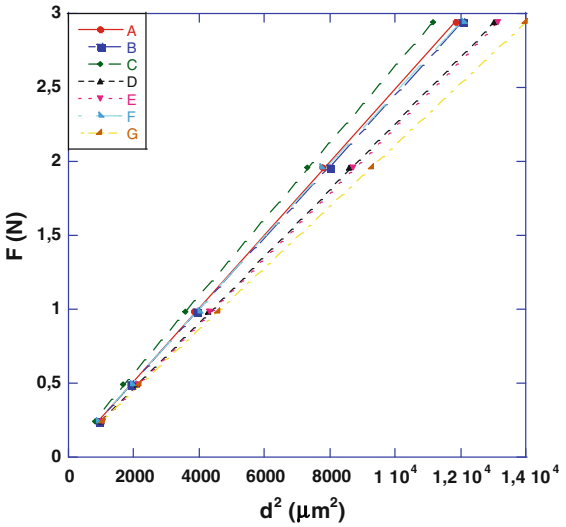

Fig. 9 Graph of the applied load against the square of the diagonal length for the samples

Table 8 Best-fit results of experimental data according to *HK* approach

Samples	$A_{1HK} \times 10^{-5}$	W_{HK} (N)	Load independent H_{HK} (GPa)	H_v (GPa)
A	29.99	0.019	0.556	0.560–0.566
B	28.93	0.018	0.536	0.541–0.543
C	26.02	0.042	0.482	0.488–0.495
D	22.46	0.018	0.416	0.418–0.422
E	22.28	0.014	0.413	0.414–0.417
F	24.29	0.025	0.450	0.450–0.458
G	20.78	0.030	0.385	0.390–0.392

(reversible) deformation due to the absence of the elastic recovery in a material and so the indenter easily penetrates into the material [53, 54]. In this case, the indentation diagonal length is changed by an effective load $F_{eff} = F - W_{HK}$ instead of the applied indentation test load (F) and can be found by means of the following relation:

$$F - W_{HK} = A_{HK} d^2 \tag{16}$$

where A_{HK} is the load independent constant. Here, the A_{HK} and W parameters can be extracted from the linear graphs of F against d^2 (Fig. 9). The obtained values of A_{HK}, W_{HK} and H_{HK} values are clearly given in Table 8. As seen from the table that all the W_{HK} values are noted to be positive as a consequence of the presence of both elastic and plastic deformation in the materials under the applied indentation load, pointing out the ISE feature of the samples [37, 49]. The long and short of it is that the applied load is not adequate to produce seriously the plastic deformation in the materials.

Furthermore, the corresponding H_{HK} values of the bulk Bi-2212 samples are calculated from the equation as follow:

$$H_{HK} = 1,854.4 A_{HK} \tag{17}$$

The calculated H_{HK} values are gathered in Table 8. One can see from the table that all the H_{HK} values in the present model are found to be much closer to the true microhardness in the saturation region as compared to those of the other models. Hence, it is necessary to underline that the *HK* approach is the most successful model to understand the mechanical characteristics of the bulk *Bi-2212* superconducting samples, exhibiting the *ISE* behaviour.

Based on the model evidences, the major conclusions are arranged as below.

- All the samples obey the typical ISE feature.
- The G sample presents the best mechanical properties for technological and industrial applications while the A sample presents the worst properties. This difference stems from the degradation of the connectivity between superconducting grains.
- According to the literature researches, the value of the load independent should be close to the saturation (plateau) region [38, 55]. Among the available methods, the HK approach is the best fitted model to the load dependence of microhardness values (Table 9). Thereby, this model is found to be the most successful to describe the mechanical properties of the bulk Bi-2212 superconducting materials, exhibiting the ISE behavior.

Table 9 The results of load dependent Vickers microhardness at the plateau region and load independent hardness values calculated using *PSR*, *MPSR*, *EPD* and *HK* approaches

Samples	H_v (GPa) (plateau region)	H_{PSR} (GPa)	H_{MSPR} (GPa)	H_{EPD} (GPa)	H_{HK} (GPa)
A	0.560–0.566	0.547	0.532	0.535	0.556
B	0.541–0.543	0.479	0.530	0.474	0.536
C	0.488–0.495	0.463	0.455	0.464	0.482
D	0.418–0.422	0.408	0.408	0.408	0.416
E	0.414–0.417	0.407	0.406	0.407	0.413
F	0.450–0.458	0.439	0.427	0.439	0.450
G	0.390–0.392	0.371	0.384	0.363	0.385

4 Conclusion

In this study, the influence of annealing ambient on the electrical, microstructural, mechanical and superconducting properties of the Bi-2212 superconducting materials prepared by normal solid-state reaction technique is surveyed by means of XRD, dc resistivity, SEM and Vickers microhardness measurements. The onset-offset critical transition temperature, variation of transition temperature, hole carrier concentration, crystal structure, texturing (crystal plane alignment), crystallinity, cell parameter, crystallite size, specimen surface morphology, grain connectivity, grain size distribution, load dependent microhardness, elastic modulus and yield strength characteristics, being in charge of the potential technological and industrial applications, are obtained for the Bi-2212 superconducting materials. All the results indicate that the properties given above depend crucially on both the annealing time and temperature. Besides, we theoretically analyze the load independent microhardness values to determine the sample behavior under the applied load with the aid of the available methods such as Meyer's law, elastic/plastic deformation, proportional sample resistance and Hays–Kendall approach. The long and short of the major findings determined from this work are as follows:

- The electrical, microstructural, mechanical and superconducting properties of the samples are found to improve up to the annealing temperature of 840 °C beyond which they degrade considerably and in fact reach the minimum points at annealing temperature of 850 °C. Thus, the best annealing ambient is observed to be 840 °C for 72 h to promote the velocity of Bi-2212 superconducting phase formation.
- The T_c^{offset} and T_c^{onset} values are observed to be in a range of 58.16 K-78.90 K and 77.87–84.79 K, respectively. The Bi-2212 superconductor, subjected to the annealing process at 840 °C for 72 h, obtains both the greatest T_c^{offset} ($\approx$78.90 K) and T_c^{onset} ($\approx$84.79 K) values. On the other hand, the sample annealed at 850 °C for 24 h has the minimum values. This is attributed to the fact that the excess annealing temperature damages seriously the critical transition temperatures.
- Similarly, the XRD analysis results illustrate that the same sample has the greatest diffraction line intensities belonging to the Bi-2212 phase, crystallite size and lattice constant parameter *c*. Furthermore, the SEM experiments confirm that the same sample with the smoothest and densest surface morphology obtains the best grain connectivity between the superconducting grains and largest crystalline size distribution. This is enough to verify that why the best condition is the annealing temperature of 840 °C with the duration of 72 h.
- For the mechanical properties, the microhardness experiments show that the Vickers microhardness, elastic modulus, yield strength and fracture toughness values decrease with increasing the applied loads. This is attributed to the fact that all the samples prepared present the standard *ISE* behaviour due to the production of the elastic and plastic deformation simultaneously. In other words, the elastic recovery is dominant character on the samples. It is another interesting result that the sample produced at 840 °C for the annealing duration of 72 h obtains the minimum microhardness values.
- As for the theoretical findings examined, the results of the Hays–Kendall approach are obtained to be closer to the saturation (plateau) region as compared to other models, meaning that the *HK* model is the most successful approach for the explanation of the mechanical properties of the Bi-2212 materials studied in the present work.

References

1. H. Maeda, Y. Tanaka, M. Fukutomi, T. Asano, Jpn. J. Appl. Phys. Lett. **27**, 209 (1988)
2. J.M. Tarascon, Y. Lepage, L.H. Greene, B.G. Bagley, P. Barboux, D.M. Hwang, G.W. Hull, W.R. Makinnon, M. Giroud, Phys. Rev. B **38**, 2504 (1988)
3. N. Ghazanfari, A. Kilic, A. Gencer, H. Ozkan, Solid State Commun. **144**, 210 (2007)
4. T. Makise, S. Uchida, S. Horii, J. Shimoyama, K. Kishio, Physica C **460**, 772 (2007)
5. G. Yildirim, Y. Zalaoglu, M. Akdogan, S.P. Altintas, A. Varilci, C. Terzioglu, J. Supercond. Nov. Magn. **24**, 2153 (2011)
6. J.M. Tarason, P. Barboux, G.W. Hull, R. Ramesh, L.H. Greene, M. Giroud, M.S. Hegde, W.R. Mckinnon, Phys. Rev. B **39**, 4316 (1989)
7. V.P.S. Awana, S.K. Agarwal, R. Ray, S. Gupta, A.V. Narlikar, Physica C **191**, 43 (1992)
8. K. Koyama, S. Kanno, S. Noguchi, Jpn. J. Appl. Phys. **29**, 53 (1990)
9. H. Hilgenkamp, J. Mannhart, Rev. Mod. Phys. **74**, 485 (2002)
10. C. Autret-Lambert, B. Pignon, M. Gervais, I. Monot-Laffez, A. Ruyter, L. Ammor, F. Gervais, J.M. Bassat, R. Decourt, J. Solid State Chem. **179**, 1698 (2006)
11. Z. Wang, J.R. Engelbrecht, S. Wang, H. Ding, Phys. Rev. B **65**, 064509 (2002)
12. Q.H. Wang, J.H. Han, D.H. Lee, Phys. Rev. B **65**, 054501 (2002)
13. N.T. Mua, A. Sundaresan, N.K. Man, D.D. Dung, Bull. Mater. Sci. (2013) (in press)
14. O. Ozturk, E. Asikuzun, M. Erdem, G. Yildirim, O. Yildiz, C. Terzioglu, J. Mater. Sci. Mater. Electron. **23**, 511 (2012)
15. O. Ozturk, E. Asikuzun, G. Yildirim, J. Mater. Sci. Mater. Electron. **24**, 1274 (2013)
16. J.S. Moodera, R. Meservey, J.E. Tkaczyk, C.X. Hao, G.A. Gibson, P.M. Tedrow, Phys. Rev. B **37**, 619 (1988)
17. G. Yildirim, A. Varilci, M. Akdogan, C. Terzioglu, J. Mater. Sci. Mater. Electron. **23**, 928 (2012)

18. P.B. Allen, Y.E. Picket, H. Krakauer, Phy. Rev. B **37**, 7482 (1988)
19. S. Martin, M. Gurvitch, C.E. Rice, A.F. Hebard, P.L. Gammel, R.M. Fleming, A.T. Fiory, Phys. Rev. B **39**, 9611 (1989)
20. D.M. Newns, P.C. Pattnaik, C.C. Tsuei, Phys. Rev. B **43**, 3075 (1991)
21. K. Levin, J.H. Kim, J.P. Lu, Q. Si, Physica C **175**, 449 (1991)
22. P.A. Lee, N. Read, Phys. Rev. Lett. **58**, 2691 (1987)
23. M. Dogruer, G. Yildirim, A. Varilci, C. Terzioglu, J. Alloy Compd. **556**, 143 (2013)
24. M. Dogruer, Y. Zalaoglu, A. Varilci, C. Terzioglu, G. Yildirim, O. Ozturk, J. Supercond. Nov. Magn. **25**, 961 (2012)
25. J.H. Koo, G. Cho, J. Phys.: Condens. Matter **15**, 729 (2003)
26. A.I. Abou-Aly, R. Awad, A.M. Hafez, A.A. Faraj, in *International Conference on Research Trends in Science and Technology*, vol. 91 (2002)
27. K. Kocabas, O. Ozkan, O. Bilgili, Y. Kadioglu, H. Yılmaz, J. Supercond. Nov. Magn. **23**, 1485 (2010)
28. A. Ianculescu, M. Gartner, B. Despax, V. Bley, T.H. Lebey, R. Gavrila, M. Modreanu, Appl. Surf. Sci. **253**, 344 (2006)
29. A.I. Abou-Aly, S.A. Mahmoud, R. Awad, M.M.E.J. Barakat, Supercond. Nov. Magn. **23**, 1575 (2010)
30. R.D. Mangapathi, T. Somaiah, V. Haribabu, Y.C. Venudhar, Cryst. Res. Technol. **28**, 285 (1993)
31. D. Rama Sita, Doctor of Philosophy, School of Physics University of Hyderabad, Hyderabad. http://shodhganga.inflibnet.ac.in/handle/10603/1782 (1997)
32. G. Yildirim, S. Bal, E. Yucel, M. Dogruer, M. Akdogan, A. Varilci, C. Terzioglu, J. Supercond. Nov. Magn. **25**, 381 (2012)
33. J. Gong, J. Wu, Z. Guan, J. Eur. Ceram. Soc. **19**, 2625 (1999)
34. A.A. Elmustafa, D.S. Stone, J Mech Phys Solid **5**, 357 (2003)
35. L. Arda, O. Ozturk, E. Asikuzun, S. Ataoglu, Powder Technol. **235**, 479 (2013)
36. S. Celik, O. Ozturk, E. Coskun, E. Asikuzun, K. Ozturk, M. Sarıhan, C. Terzioglu, J. Mater. Sci. Mater. Electron. (2013). doi:10.1007/s10854-013-1082-9
37. R. Awad, A.I. Abou-Aly, M. Kamal, M. Anas, J. Supercond. Nov. Magn. **24**, 1947 (2011)
38. K. Sangwal, Mater. Chem. Phys. **63**, 145–152 (2000)
39. Y. Zalaoglu, E. Bekiroglu, M. Dogruer, G. Yildirim, O. Ozturk, C. Terzioglu, J. Mater. Sci. Mater. Electron. (2013). doi:10.1007/s10854-013-1098-1
40. S. Cavdar, E. Deniz, H. Koralay, O. Ozturk, M. Erdem, A. Gunen, J. Supercond. Nov. Magn. (2012). doi:10.1007/s10948-012-1629
41. D. Tabor, Philos. Mag. **74**, 1207 (1996)
42. U. Kolemen, O. Uzun, M. Yilmazlar, N. Guclu, E. Yanmaz, J. Alloy Compd. **415**, 300 (2006)
43. N.H. Mohammed, A.I. Abou-Aly, I.H. Ibrahim, R. Awad, M. Rekaby, J. Alloy Compd. **486**, 733 (2009)
44. H. Li, R.C. Bradt, J. Mater. Sci. **28**, 917 (1993)
45. E. Asikuzun, O. Ozturk, H.A. Cetinkara, G. Yildirim, A. Varilci, M. Yilmazlar, C. Terzioglu, J. Mater. Sci.: Mater. Electron. **23**, 1001 (2012)
46. J.B. Quinn, G.D. Quinn, J. Mater. Sci. **32**, 4331 (1997)
47. J. Gong, J. Wu, Z. Guan, J. Eur. Ceram. Soc. **19**, 2625 (1999)
48. M.L. Tarkanian, J.P. Neumann, L. Raymond, in *The Science of Hardness Testing and Its Research Application*, ed. by J.H. Westbrook, H. Conrad (American Society for Metals, Metal Park, OH, 1973), pp. 187–198
49. Q. Ma, D.R. Clarke, J. Mater. Res. **10**, 853 (1995)
50. F. Fröhlich, P. Grau, W. Grellmann, Phys. Status Solidi (a) **42**, 79 (1977)
51. W.C. Oliver, R. Hutchings, J.B. Pethica, in *Microindentation Techniques in Materials Science and Engineering*, ed. by P.J. Blau, B.R. Lawn (ASTM, Philadelphia, PA, 1986)
52. B.D. Michels, G.H. Frischat, J. Mater. Sci. **17**, 329 (1982)
53. C. Hays, E.G. Kendall, Metallography **6**, 275 (1973)
54. M. Yilmazlar, O. Ozturk, O. Gorur, I. Belenli, C. Terzioglu, Supercond. Sci. Technol. **20**, 365 (2007)
55. G.P. Upit, S.A. Varchenya, Phys. Status. Solidi B **17**, 831 (1966)